10660 *J. Phys. Chem. A* **2003,** *107,* 10660−10666

Nonlinear-Infrared Responses of the N−H Mode of Pyrrole in Carbon Tetrachloride by Heterodyned and Stimulated Echoes†

Jianxin Chen, Jaehun Park, and Robin M. Hochstrasser*

Department of Chemistry, University of Pennsylvania, Philadelphia, Pennsylvania 19104-6323

Received: April 21, 2003; In Final Form: July 10, 2003

Three pulse infrared nonlinear studies with 100 fs pulses at 3 μm of the N−H mode of pyrrole in carbon tetrachloride were carried out in various experimental configurations including integrated transient gratings, polarized pump−probe, heterodyned three pulse echoes, and time integrated three pulse echoes. Essential features of the N−H dynamics were obtained from the measured properties that include the population relaxation time ($T_1 = 81 \pm 15$ ps), the orientational diffusion coefficients ($D_\perp = (9.18 \pm 1.09) \times 10^{10}$ s^{-1}, $D_\parallel = (3.23 \pm 0.71) \times 10^{11}$ s^{-1}), and the N−H vibrational frequency correlation function expressed as a sum of three exponentials with correlation times 18 fs, 4.4 ps, and >10 ps.

Introduction

A very important challenge for physical chemistry is the development of methods that determine the time dependence of structural changes in complex systems. Already there have been significant advances in time-dependent X-ray diffraction[1−3] and NMR probes of equilibrium dynamics.[4] In this regard multidimensional infrared spectroscopy, 2D and 3D IR, can be expected to contribute significantly,[5−22] complementing the knowledge on average structures obtained by the more established methods of structural biology and their time-dependent variants. The backbones of protein structures are the polypeptides whose amide units, −NHCH(R)CO−, have infrared spectra that are ultrasensitive to the details of the many possible secondary structures that exist in proteins. The 2D IR method exposes much more information regarding the potential surfaces of polypetides than conventional FTIR spectroscopy because it accesses anharmonic contributions directly, but the interpretation of the results depends on having a deeper understanding of the dynamics of vibrational states than can be obtained from pump−probe experiments. Already a few nonlinear-IR spectroscopic investigations have been carried out on the amide-I and amide-II transitions of polypeptides and peptides: these transitions involve mainly the carbonyl stretching mode and in-plane CNH bending modes. Another structure sensitive vibration of the peptide group is the amide-A mode which is mainly the N−H stretching motion. Recently the first series of experiments using dual frequencies in 2D IR were used to examine the coupling between the amide-I and amide-A modes.[22] However, knowledge of the dynamics of N−H modes in peptides and in model systems has proved to be relatively scanty so we began a series of experiments to begin to fill this gap.

Nonlinear-infrared spectroscopy can provide knowledge of all the relaxation processes including some that do not manifest themselves in the linear spectral line shapes. The $v = 0 \rightarrow v = 1$ transition line shape is determined by the overall rotation of the molecule, population relaxation time T_1, and vibrational frequency correlation function. The experimental line shape is not a very useful determinant of this correlation function[23,24] because it provides experimental data only along one axis, either frequency or time, and the line shape function is usually too complex to be described by a few parameters. The third-order nonlinear-IR experiments provide data along three axes in principle, and even 2D IR obtains a square grid of data points. These factors result in the correlation function being much better determined than by linear methods. The nonlinear experiments probe levels beyond $v = 0$ and $v = 1$ and so generate relaxation properties that are not part of the IR line shape. Furthermore by judicious choice of phase matching conditions and pulse sequences, the nonlinear signal can be chosen to emphasize different characteristics of the dynamics and of the correlation function by means of the pump−probe, transient grating, and two or three pulse photon echo experimental arrangements.[11,17,23,25−30]

The N−H vibration in many model systems including peptides is a mode that is localized on essentially two atoms, and its structural sensitivity is related to the shifts that occur on hydrogen bonding. This localized picture is confirmed by force field calculations of modes and frequencies and by isotope shifts.[31] In systems with multiple N−H modes the excitations may become delocalized as a result of through space interactions which would be understood using molecular exciton methods. The N−H potential is nevertheless relatively anharmonic so the 2D IR spectra have a character different from those obtained for the C═O modes.[19,22] Furthermore hydrogen bonding is known to have a profound influence on the N−H vibrational dynamics. For example the H-bonding of pyrrole significantly alters the vibrational relaxation of the N−H excitations[32] as does the interactions between pyrrole molecules.[33−35] In this paper we examine the infrared nonlinear responses of pyrrole in a non-hydrogen-bonding environment. Pyrrole is chosen in this medium because it is known to have a relatively long population relaxation time compared with the inverse of its linear-IR spectral line width. Therefore, the line width is determined largely by reorientation and by the frequency correlation function, while the solvent, carbon tetrachloride, represents a relatively inert medium for the N−H bond in which monomers of pyrrole can be characterized.

---

† Part of the special issue "Charles S. Parmenter Festschrift".

* Corresponding author. E-mail: hochstra@sas.upenn.edu. Fax: 215-898-0590.

10.1021/jp030468z CCC: $25.00

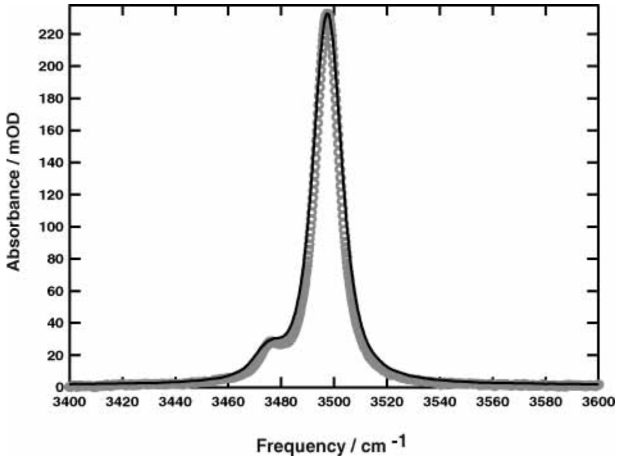

Figure 1. Linear-IR absorption spectrum (circles) of pyrrole in CCl_4. The solid line shows the spectrum obtained from the global fit of the photon echo signals and linear spectrum.

Experimental Methods

The experiments were based on the generation of pulses in the 3 μm region by femtosecond IR optical parametric amplification (OPA). A single-filament white light continuum was amplified through a two stage KTP ($KTiOPO_4$, type II, 3 mm crystal thickness) amplifier, pumped by a home-built 1 kHz Ti:sapphire regenerative amplifier/Murnane-Kaptein oscillator combination, producing pulses with energy of 320 μJ and a pulse width of 100 fs. The OPA output was chirped when driven by shorter pulses. The output beam of OPA was collimated by a curved mirror and filtered by a long-pass germanium filter. A typical pulse duration of 110 fs, a bandwidth of 140 cm^{-1}, and an energy 4.5 μJ were obtained in the 2700−3600 cm^{-1} range.

The IR pulses were split into three equal-intensity excitation beams (k_1, k_2, k_3) and a fourth weak local oscillator beam (k_{LO}). The excitation beams were focused on the sample in the geometry of a box configuration.[14] The generated third-order field in the $-k_1 + k_2 + k_3$ phase-matched direction[11,14] was directly integrated on a liquid-N_2-cooled HgCdTe detector for the stimulated photon echo experiment. It was combined with the k_{LO} beam on the detector for the heterodyned experiment.

The optical path lengths of the k_1, k_3, k_{LO} pulses were varied separately by computer-controlled delay lines. The time delay τ separated the k_1 and k_2 pulses, T referred to the delay between k_2 and k_3, and t referred to the separation between the k_3 and k_{LO} pulses.

The pump−probe experiments were carried on the same apparatus. One of three beams was selected as the pump, and another was attenuated to act as the probe. The probe was dispersed and projected onto a 32 channel MCT array detector.

Sample. Pyrrole was purchased from Aldrich and distilled before use. Pyrrole in CCl_4 FT-IR absorption spectra (NH stretching region) were recorded on a Perkin-Elmer Spectrum 2000 Explorer FT-IR spectrometer with 1 cm^{-1} resolution (Figure 1). The concentration of the solution was 38 mM, and the OD was ∼0.3. The sample was placed in a cell between CaF_2 windows spaced by 250 μm.

Description of Nonlinear Infrared Signals. To establish the essential parameters of the vibrational dynamics of the N−H stretching mode of pyrrole a number of different nonlinear-infrared experimental approaches were used. Here we introduce the vibrational response functions associated with these configurations. These, and the analogous optical response functions,[36] have been discussed in detail previously[7,11,17,37] so they are only summarized here.

The response functions for signals generated by three pulses are written as $G^p_{ijkl}(\tau,T,t)$, where τ and T are the intervals between the first and the second two pulses while t is the time elapsed after the third pulse. The indices i, j, k, and l refer respectively to the polarizations of the first, second, third, and generated fields. When the orientational and vibrational motions are not coupled, the response function can be written as the product of an orientational O_{ijkl} and an isotropic vibrational part R_p corresponding to a particular pathway, designated p, in Liouville space, so that

$$G^p_{ijkl}(\tau,T,t) = \mathrm{O}_{ijkl}(\tau,T,t)R_p(\tau,T,t) \tag{1}$$

Pyrrole is planar and close to being a symmetric rotor and a symmetric diffuser for which the volumes swept out by rotation around the two principal in-plane axes of diffusion ($D_\perp$) are similar. The unique axis, perpendicular to the molecular plane, is ascribed the diffusion coefficient $D_{||}$. The effect of orientational dynamics on the signals is caused by the rotation of the vibrational transition dipole moment that is parallel to the N−H bond. Standard methods[38] can be used to obtain the relevant orientational contributions to the response function for this type of diffuser:

$$\begin{aligned}\mathrm{O}_{zzzz}(\tau,T,t) &= \\ &1/9\mathrm{e}^{-(D_\perp+D_{||})(t+\tau)}[1 + 0.2\mathrm{e}^{-6D_\perp T} + 0.6\mathrm{e}^{-(2D_\perp+4D_{||})T}] \\ \mathrm{O}_{zzxx}(\tau,T,t) &= \\ &1/9\mathrm{e}^{-(D_\perp+D_{||})(t+\tau)}[1 - 0.1\mathrm{e}^{-6D_\perp T} - 0.3\mathrm{e}^{-(2D_\perp+4D_{||})T}]\end{aligned} \tag{2}$$

The isotropic responses $R_p(\tau,T,t)$ are different for each Liouville pathway, p,[36] One can use double-sided diagrams[39] to specify these pathways in the space of the reduced density matrix, but we will refer to the relaxation functions $\mathscr{T}_p(ab|cd|ef)$ to designate the density matrix elements that characterize the system after the first (ρ_{ab}), second (ρ_{cd}), and third (ρ_{ef}) pulses of a sequence. In an earlier paper[17] the explicit forms for the $\mathscr{T}_p(ab|cd|ef)$ based on the cumulant expansion[36] were given. The overall responses include the $\mathscr{T}$'s and the oscillatory frequency factors:

$$R_p(\tau,T,t) = \mathrm{i}\mu^4\mathscr{T}_p(ab|cd|ef)\mathrm{e}^{\mathrm{i}(\omega_{\mathrm{ba}}\tau+\omega_{\mathrm{dc}}T+\omega_{\mathrm{fe}}t)} \tag{3}$$

Here μ^4 is a transition dipole factor that will be introduced explicitly later. The relaxation functions depend on the vibrational frequency correlation functions and on the population relaxations of the various states involved in the particular pathway. When the incident pulses are short enough to encompass both the $v = 0 \rightarrow v = 1$ and $v = 1 \rightarrow v = 2$ transitions of the N−H oscillator, which are separated by ca. 140 cm^{-1}, the response functions involved for each of the N−H bands in the linear spectrum are the same as those used previously for integrated echo experiments on N_3^{-} [23] and acetic acid,[38] namely:

$$\begin{aligned}\sum_{p=1}^{3}R_p &= \\ &\mathrm{i}\mu_{01}^4\mathrm{e}^{\mathrm{i}\omega_{10}(\tau-t)}(2\mathscr{T}_1(01|00|10) - \alpha\mathscr{T}_3(01|11|1+1,1)\mathrm{e}^{\mathrm{i}\Delta t}) \\ \sum_{p=4}^{6}R_p &= \\ &\mathrm{i}\mu_{01}^4\mathrm{e}^{\mathrm{i}\omega_{10}(-\tau-t)}(2\mathscr{T}_4(10|00|10) - \alpha\mathscr{T}_6(10|11|1+1,1)\mathrm{e}^{\mathrm{i}\Delta t})\end{aligned} \tag{4}$$

where the $p = 1-3$ and $p = 4-6$ represent the rephasing and nonrephasing response functions, respectively, the $v = 2$ state is written as $(1 + 1)$, Δ is the diagonal anharmonicity, and $\omega_{10} = \omega(v = 1) - \omega(v = 0)$ and $\omega_{00} = \omega_{11} = 0$. The factor α is the ratio of the $1 \rightarrow 1 + 1$ and $0 \rightarrow 1$ transition strengths, μ_{12}^2/μ_{01}^2, which for a harmonic oscillator is precisely 2. The double Fourier transform of this response gives spectral peaks at ω_{10}, along τ, and $\omega_{10} - \Delta$ along t. To illustrate the typical content of the $\mathscr{T}$'s[14,17,23] we give the form of these echo relaxation terms:

$$\mathscr{T}_2(01|11|10) = \mathscr{T}_1(01|00|10) = \mathrm{e}^{-(t+2T+\tau)/2T_1(v=1)}\mathrm{e}^{-g(\tau)+g(T)-g(t)-g(\tau+T)-g(t+T)+g(t+T+\tau)}$$

$$\mathscr{T}_3(01|11|1+1,1) = \mathscr{T}_2(01|11|10)\mathrm{e}^{-t/2T_1(v=2)}$$

$$\mathscr{T}_5(10|11|10) = \mathscr{T}_4(10|00|10) = \mathrm{e}^{-(t+2T+\tau)/2T_1(v=1)}\mathrm{e}^{-g(\tau)-g(T)-g(t)+g(\tau+T)+g(t+T)-g(t+T+\tau)}$$

$$\mathscr{T}_6(10|11|1+1,1) = \mathscr{T}_5(10|11|10)\mathrm{e}^{-t/2T_1(v=2)} \qquad (5)$$

Here the T_1's are the population relaxation times for the indicated states and $g(t)$ is related to the correlation function of the vibrational frequency fluctuation:[36,40,41]

$$g(t) = \int_0^t \mathrm{d}t_1 \int_0^{t_1} \mathrm{d}t_2 \langle \delta\omega(t_1)\delta\omega(t_2)\rangle \qquad (6)$$

These relationships assume there are no rapid fluctuations in the anharmonicity and that the inhomogeneous distributions of the $0 \rightarrow 1$ and $1 \rightarrow 2$ transitions are fully correlated. Both experiments[11,42] and theory[14,17,23,43] suggest that this is a reasonable set of assumptions for a single oscillator. In the case of pyrrole, the N−H region of the linear spectrum consists of two bands (a and b) so that additional cross terms must be included in the response:

$$\mathscr{T}_p(01_a|1_b1_a|1_b0),\quad \mathscr{T}_p(01_b|1_a1_b|1_a0),\quad \mathscr{T}_p(01_a|1_b1_a|1_a+1_b,0) \text{ and } \mathscr{T}_p(01_b|1_a1_b|1_a+1_b,0)$$

The total contribution from these terms is quite small for pyrrole because the coupling between a and b is small as indicated by their relative intensities in the linear spectrum shown in Figure 1. It is important to point out that these four cross terms would vanish if there were no direct coupling between the modes or no indirect coupling between them through the solvent, because in that case $\omega_{1_a+1_b,1_a} = \omega_{1b}$, the population relaxation of the state $(1_a + 1_b)$ would be the sum of the relaxation rates of 1_a and 1_b, and the joint third-order response would vanish.

The time integrated three-pulse echo signal, known as the stimulated echo, is given by:

$$I_{\mathrm{SE}}(\tau,T) = \int_0^\infty \left|\sum_p G^p_{ijkl}(\tau,T,t)\right|^2 \mathrm{d}t \qquad (7)$$

where the sum is over all the Liouville paths involved in the response. The vibrational frequency correlation function is obtained by least-squares fitting a two-dimensional grid of experimentally determined $I_{\mathrm{SE}}(\tau,T)$ to models for the correlation function. While this correlation function is in principle contained in the linear-IR spectrum, there is usually insufficient experimental information to extract it.[23,24] The individual scans of $I_{\mathrm{SE}}(\tau,T)$ along τ do not necessarily peak at $\tau = 0$, giving rise to the so-called echo peak shift which diminishes as T increases, and the system loses memory of the initially excited inhomogeneous distribution of frequencies.[18,23,25,26,29,44]

The heterodyned experiments basically measure the generated electric fields from the responses given above. In principle the heterodyned function of three time intervals incorporates all third-order experiments including pump probe, transient gratings, and echoes carried out with the same pulses. From Maxwell's equations, we find that the complex generated field is proportional to the imaginary part of the macroscopic polarization, which in turn is proportional to the response function. The detected field in a heterodyne experiment is the real part of the complex generated field which corresponds to the imaginary part of the response function, namely $\mathrm{Im}\{G^p_{ijkl}(\tau,T,t)\}$.

In all of the foregoing formulations the assumption has been made that the bandwidth of the laser pulses is large enough to bracket all the possible states of the system of N−H vibrators. Since in practice the pulses have limited spectral width, the actual signals must involve a convolution with the incident laser pulses. For example, the anharmonicity of the N−H mode is sufficiently large that pulses could be chosen to pick out only the first term in eq 4 yet they were still short enough to resolve some of the dynamics associated with the $v = 0/v = 1$ two-level system.

Results and Discussion

The linear spectrum of pyrrole, shown in Figure 1, consists of two bands, a main band at 3495 cm^{-1} having a full width at half-maximum of 11 cm^{-1} corresponding to "free" N−H and a band at 3473 cm^{-1} having 7% of the strength of the main band. This weak band could be a Fermi resonance or a hot band. Grubbs et al.[32] identified this small band as "self-associated" pyrrole−pyrrole complex, yet we have seen no change in the ratio of two peaks on diluting the sample from 45 mM to 200 μM. In the gas phase there is a weak satellite to the main N−H stretch displaced to lower frequency by 24 cm^{-1} which is definitively assigned as a hot band involving the N−H bend at 475 cm^{-1}.[45] These gas-phase spectra provide no evidence for the existence of a strong Fermi resonance in the region of the fundamental. The Fermi resonance and hot band are expected to have quite different effects on the overall nonlinear response and therefore should be distinguishable by nonlinear spectroscopy as discussed in more detail below.

The predicted form of the heterodyned broad band echo signal is given by eq 4 for each oscillator. The Fourier transform of this response gives, by inspection, two peaks for each oscillator (a and b), one peak at ω_{10} and the other at $\omega_{10} - \Delta$. The results are shown in Figure 2 which indicates that $\Delta_{\mathrm{a}} = 139$ cm^{-1} for the main N−H stretch of pyrrole[32,45–48] and $\Delta_{\mathrm{b}} = 142$ cm^{-1} for the weak shoulder for $\tau = 300$ fs and $T = 0$ fs. Figure 2a shows the observed heterodyned signal of the generated photon echo field as a function of the local oscillator delay time with respect to the third laser pulse. It shows clear beatings with a period of about 240 fs. Since these are from the superposition of two emitted fields (nonassociated N−H and anharmonically shifted free induction decays) which have a frequency difference of about 140 cm^{-1}, one cannot see these beatings in the response of the two-level systems excited with narrower bandwidth pulses (as in Figures 3 and 4). The Fourier transform of the heterodyned echo signals give the frequency spectra of the generated echo fields, Figure 2b. This spectrum shows four peaks: the main N−H stretching peak ($v = 0 \rightarrow v = 1$) and its anharmonically shifted partner ($v = 1 \rightarrow v = 2$) and the weak N−H band and its anharmonically shifted partner. These anharmonically shifted peaks are also clearly seen for $\tau = 300$ fs and $T = 300$ fs (data

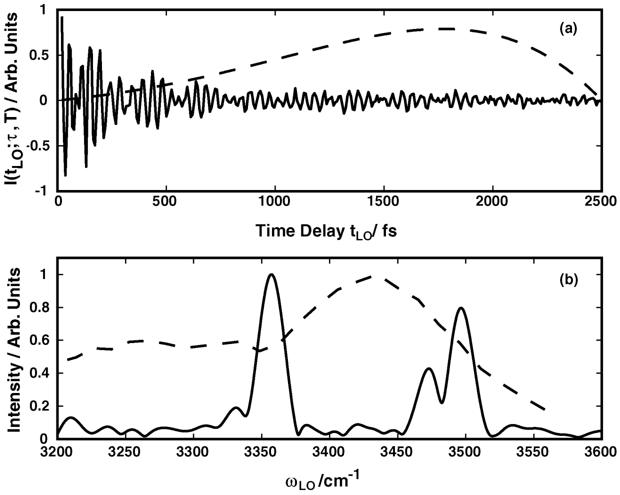

Figure 2. (a) Heterodyned broad band signal of the generated photon echo field for $T = 0$ fs, $\tau = 300$ fs as a function of t_{LO}, and window function with $\lambda = -2.4$ (dashed) and (b) the Fourier transform of this signal after application of the window function to the heterodyned signal and OPA spectra (dashed).

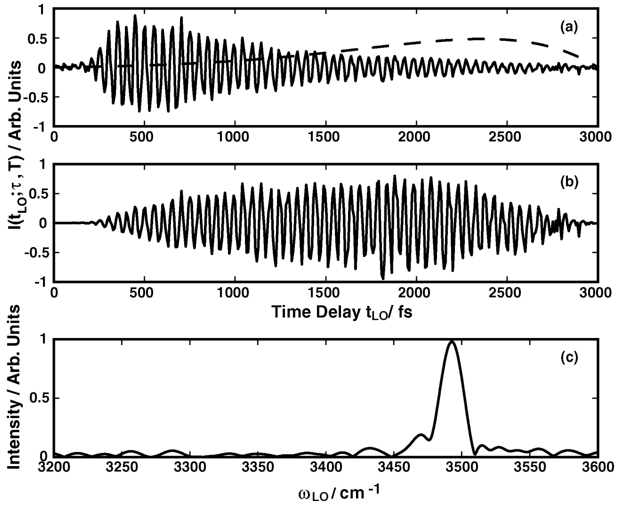

Figure 3. (a) Unprocessed heterodyned signal of the generated photon echo field for $T = 400$ fs, $\tau = 400$ fs as a function of t_{LO}, and the window function with $\lambda = -4$ (dashed), (b) the heterodyned signal after applying the window function, and (c) the Fourier transform of this signal.

not shown), and the data provide the anharmonicities, Δ_a and Δ_b. Although a broader spectral width was used to encompass both the $v = 0 \rightarrow v = 1$ and $v = 1 \rightarrow v = 2$ transitions of the N−H, the excitation pulses are still not sufficiently broad to generate the same signals for each transition. Therefore the relative intensities of the four Fourier transformed peaks are significantly influenced by our laser pulses. The intensity of the weak band ($v = 0 \rightarrow v = 1$) at 3473 cm^{-1} was overemphasized compared with the main band at 3495 cm^{-1} due to the larger laser intensity at 3473 cm^{-1}, but even after considering the convolution with the laser pulses, the weak N−H stretching band is still 1.7 times larger than expected. This gives some idea of the experimental error in the intensity measurements. The intensity ratio of the pair of anharmonically shifted peaks ($v = 1 \rightarrow v = 2$) matches reasonably with expectations from the linear spectrum and from the ratio obtained from the two level response with a narrower pulse in the $v = 0 \rightarrow v = 1$ region. On the basis of the double-sided Feynman diagrams,[14] two diagrams result in emission from the 1−0 coherence at

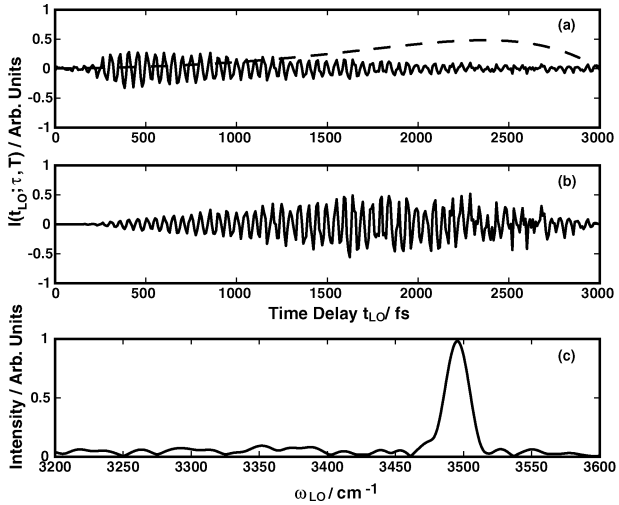

Figure 4. (a) Unprocessed heterodyned signal of the generated photon echo field for $T = 400$ fs, $\tau = 1500$ fs as a function of t_{LO}, and the window function with $\lambda = -4$ (dashed), (b) the heterodyned signal after applying the window function, and (c) the Fourier transform of this signal.

center frequency 3495 cm^{-1} and one diagram in emission from the 2−1 coherence centered at 3356 cm^{-1}; however, since the ratio $\mu_{12}{}^2/\mu_{01}{}^2$ is precisely 2 for a harmonic oscillator, the emission intensities for the 1−0 and 2−1 coherences are expected to be about same. Figure 2b shows that the intensity of the anharmonically shifted peak is 20% larger than the free N−H main peak, which represents reasonably good agreement.

The two-level response is given by the first part of eq 4 for each oscillator which yields the heterodyned signal and its Fourier transform shown in Figure 3 for $\tau = 400$ fs and $T = 400$ fs and Figure 4 for $\tau = 1500$ fs and $T = 400$ fs. These Fourier-transformed spectra show peaks at 3495 and 3473 cm^{-1}. However, they have contributions from scattered light. Applying an appropriate window function to the data before Fourier transforming can reduce these wings and improve the signal-to-noise ratio.[11,12] A window function, $h(t_{LO}) = ce^{-\lambda t/t_{max}} \sin(\pi t/t_{max})$, was used, where t_{max} is the largest t that signal was collected and c is a constant. This window function is shown in Figures 3a and 4a (dashed) for $\lambda = -4$, and Figures 3b and 4b show its effect on the unprocessed data. As mentioned above, although pulses were chosen to pick out only the first term in eq 4, information was still not enough to resolve some of the dynamics associated with the $v = 0/v = 1$ two-level system using a 1-D heterodyned echo experiment. The 2-D heterodyned photon echo experiment, which is not dealt with in this paper, could give more information about the dynamics including coupling between two oscillators.

If we return to the issue of Fermi resonance versus hot band, the results of the photon echo suggest the hot band interpretation is the correct one. The Fermi resonance would be associated with some combination of modes that closely matches the N−H frequency. The excitation of the N−H mode on the basis of this combination state would not involve the full anharmonicity of the N−H mode. However, the experiment measures $\Delta_b = 142$ cm^{-1} for this transition, which is almost equal to the value of 139 cm^{-1} obtained for Δ_a. The similarity between these two values strongly suggests that the final state of the transition involved in the echo of the weak transition contains two quanta of the N−H mode, thereby favoring a hot band interpretation. This conclusion is also consistent with the absence of the combination tone 1a + 1b in any of the spectra: for example

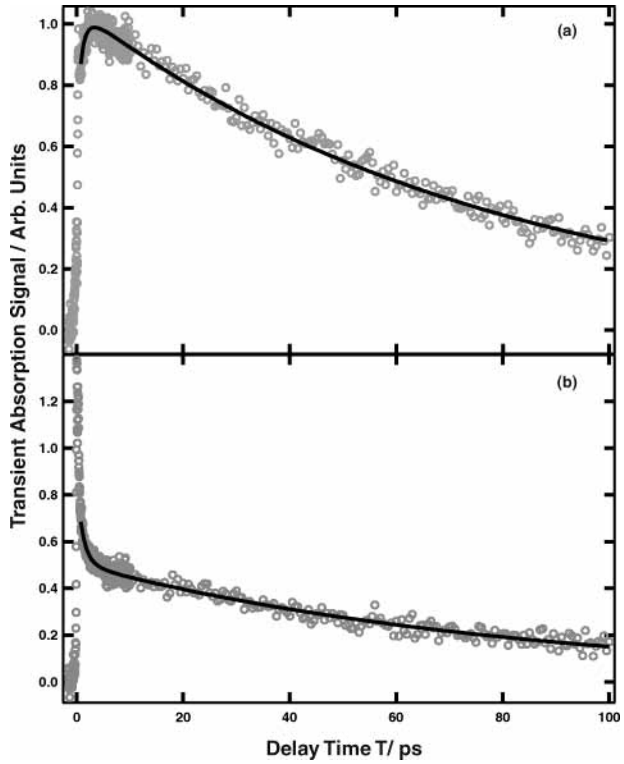

Figure 5. Transient absorption decay (circles) of pyrrole in CCl_4: (a) perpendicular polarization; (b) parallel polarization. Solid lines represent fits of experimental data to double-exponential decay of rotational diffusion model (see eq 2).

for two coupled modes we would have seen this combination in the echo spectrum of Figure 2 in accordance with the predictions discussed above. These results imply that the echo signals from the strong and weak components involve independent sets of Liouville paths, one set initiating on a population of the ground state and the other on a population of a mode at 475 cm^{-1}. The signal field on the detector is therefore the sum of two independent signals with no field generated jointly by both the main and subsidiary peaks.

The pump probe signal was used to obtain the value of $T_1(\upsilon = 1)$ and the rotational diffusion coefficient. The measured value of $T_1 = 81 \pm 15$ ps was comparable with the value $T_1 = 60 \pm 10$ ps reported previously[32] (see Figure 5). The value of $T_1(\upsilon = 2)$ was assumed to be $T_1(\upsilon = 1)/2$ in accordance with a model for a harmonic vibrator that is linearly coupled to a bath.

The anisotropy data was fitted to two exponentials which were assumed to measure the combinations of $D_{\|}$ and $D_{\perp}$ given above. The diffusion coefficients obtained from the fit are $D_{\perp} = (9.18 \pm 1.09) \times 10^{10}$ s^{-1} and $D_{\|} = (3.23 \pm 0.71) \times 10^{11}$ s^{-1}. Using known rotational constants,[48] the orientational relaxation times for free rotor[38] are estimated to be 0.331 (axis *a*), 0.334 (axis *b*), and 0.471 ps (axis *c*). From the data of bond lengths and angles of pyrrole and standard van der Waals radii,[48] we obtain semiaxis lengths of $a = 3.08$ Å, $b = 3.21$ Å, and $c = 1.7$ Å. In the "stick" hydrodynamic limit, with pyrrole approximated as an oblate symmetric diffuser with its vibrational transition perpendicular to the symmetry axis (axis *c*), the diffusion coefficients are found to be $D_{\perp} = 9.12 \times 10^9$ s^{-1} and $D_{\|} = 7.38 \times 10^9$ s^{-1}. These coefficients are 10 times smaller than those obtained from experiment. In the "slip" hydrodynamic limit,[49,50] the principal diffusion coefficients of pyrrole are calculated to be $D_a = 4.10 \times 10^{10}$ s^{-1}, $D_b = 5.10 \times 10^{10}$ s^{-1}, and $D_c = 1.49 \times 10^{12}$ s^{-1}. For an oblate symmetric diffuser approximation, $D_{\perp} = D_a \approx D_b$ and $D_{\|} = D_c$. The slip rotational diffusion time around the symmetry axis (axis *c*) is faster than the free rotor decay. So some inertial dynamics is predicted to be involved in the rotational motion.[51]

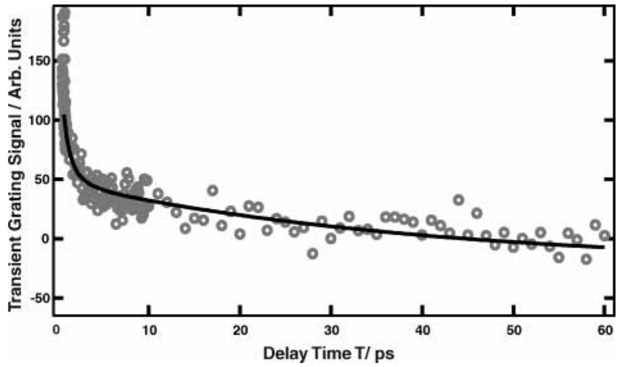

Figure 6. Integrated transient grating signal decay (circles) of pyrrole in CCl_4 as a function of *T*. The solid line represents a fit of experiment data to double-exponential decay of rotational diffusion model (see eq 2).

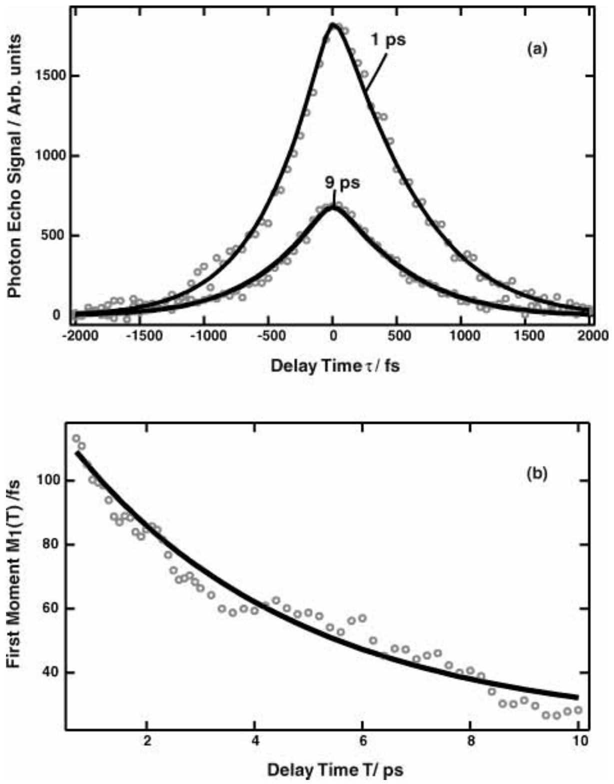

Figure 7. (a) Stimulated photon echo signal (circles) of pyrrole in CCl_4 as a function of *t* in the $-k_1 + k_2 + k_3$ direction for two selected values of *T*. The solid lines represent a global fit of the 59 scans (from 700 fs to 10 ps) to the model correlation function. (b) First moment $\mathbf{M}_1(T)$ of the data measured in the $-k_1 + k_2 + k_3$ direction of pyrrole in CCl_4 (circles). The solid line is the first moment $\mathbf{M}_1(T)$ obtained from the global fit.

The rotational dynamics was also seen clearly in the integrated transient grating echo signal shown in Figures 6. The integrated echo signal corresponds to the integral over *t* of the absolute square of the first term in eq 4 with the orientational response function (eq 2) for $\tau = 0$.

The three-pulse integrated photon echo is aimed at obtaining the vibrational frequency correlation function as displayed in eq 9. For each value of *T* an echo signal versus τ was obtained. Two examples such traces are shown in Figure 7a. The peak shift of the photon echo signal was measured to be about 70 fs at $T = 400$ fs. The first moment of the photon echo signal

$$M_1(T) = \int_{-\infty}^{\infty} \tau I_{\mathrm{SE}}(\tau,T)\,\mathrm{d}\tau \Big/ \int_{-\infty}^{\infty} I_{\mathrm{SE}}(\tau,T)\,\mathrm{d}\tau \qquad (8)$$

was used to measure asymmetry between the rephasing and the nonrephasing signal.[14,23] The decay of the first moment versus T was the evidence of the spectral diffusion processes in our experimental time window (see Figure 7b). The signals were simulated using eqs 1, 2, and 4 for both oscillators and integrating the absolute square of the sum of all relevant terms over the time interval t ($t \geq 0$). The collection of echo signals for 59 different values of T ranging from 700 fs to 10 ps, their normalized first moments, and the linear spectrum were globally least-squares fitted to a model function:

$$\langle \delta\omega(t_1)\delta\omega(t_2)\rangle = \sum_{k=1}^{3} A_k^{\,2} \mathrm{e}^{-t/\tau_k} \qquad (9)$$

The optimum values of A in ps^{-1} and τ in ps were $A_1 = 4.6 \pm 2.0$, $\tau_1 = 0.018 \pm 0.015$, $A_2 = 0.59 \pm 0.01$, $\tau_2 = 4.4 \pm 0.2$, and $A_3 = 0.18 \pm 0.01$, and τ_3 was larger than the delays so that A_3 represents an inhomogeneous distribution fixed on the time scale of the experiment. These parameters enabled us to simulate the linear spectrum, Figure 1, and the first moment as illustrated in Figure 7b. The agreement is excellent in both cases. The weak transition was attributed the same dynamics as the main band because its contribution to the signal is too small to permit the experimental determination of an independent correlation function.

The specification of a correlation function for the N−H vibrational frequency as a sum of three exponentials (eq 9) is somewhat arbitrary. We would expect that the correlations in the vibrational frequency of a solute in a solution would be lost gradually and not necessarily in well-separated exponential steps, although there are theoretical reasons for bimodality in the case of liquid water.[52] Therefore, other functions would also describe the limited data set that we have obtained, but the signal-to-noise ratio of the data, which decreases with increasing delay time T, is not high enough at present to justify an assessment of the appropriateness of different decay functions. The slow correlation time of 4.4 ps measured in the three-pulse echo experiments, which corresponds to that part of the vibrational frequency distribution that is not averaged by solvent fluctuations, must arise from solvent motions and might be expected to be seen in other experiments that measure the solvent spectral density. The fastest component of the correlation function satisfies $A_1\tau_1 \ll 1$ so these fluctuations motionally narrow the distribution of vibrational frequencies represented by A_1. Because the T_1 relaxation is so slow compared with the observation time scale, the decay of the correlation function should mainly involve the response of the N−H mode frequency. In the case of peptides T_1 is often a dominant mode of decay so that relaxation into other states occurs during the heterodyne signal acquisition.[12,20] The resulting coherence and population transfer causes other modes to become involved in the signals, which can then persist for time scales corresponding to the cooling of the molecule. However such is not expected to be the case here although it could not be completely ruled out as a contributor to the small long-lived component in the correlation function discussed in the next paragraph.

The 4.4 ps process is longer than the orientational relaxation time of 1.7 ps, measured by NMR[53] and Raman scattering[54] for liquid CCl_4. It is comparable to the longest time constant computed from molecular dynamics simulations of the liquid which finds values $t_1 = 4$ ps and $t_2 = 1.7$ ps.[55,56] The slowest process we see is longer than all the correlation times reported in the time dependence of the optical photon echo peak shift of a nonpolar perylene derivative in CCl_4 that was recently reported.[57] In that experiment the solvent CCl_4 exhibits relaxation time scales of 80 fs, 500 fs, and 2 ps which were attributed to inertial, diffusional, and structural relaxation of the solvent, respectively. It is clear from our data that the structural relaxation of the solvent associated with pyrrole molecules stretches out to time scales that are significantly slower than expected from these results. Furthermore, there appears to be a distribution of vibrational frequencies, represented by A_3, that does not relax significantly on our experimental time scale. These results are counterintuitive for the case of a small molecule in a relatively inert, nonviscous solvent, especially one that is rotating rapidly on the time scale of the spectral diffusion, unless there is a specific solvent interaction that leads to a complex having a significant lifetime. One possibility is a weak interaction between a Cl atom and the π-electron system of pyrrole, leaving the solute the opportunity to rotate around the vertical axis without disturbing the solvent above and below the plane. There have been dynamics simulations of benzene in carbon tetrachloride that show the tendency for chlorine atoms to cluster around the π-electron "holes." These simulations also show that benzene molecules rotate three times faster about the axis perpendicular to the molecular plane.[58] Therefore, we might expect that an inhomogeneous distribution of frequencies could be maintained for times longer than the measured rotational diffusion time, which is dominated by the fast process. High-level ab initio calculations have shown that the benzene−chloroform interaction is larger than that of a hydrogen bond between two waters.[59] However the interaction between carbon tetrachloride and benzene is not short range as expected from charge-transfer effects but is long range, originating from electrostatic effects and dispersion forces.[59] Such interactions, which may also exist for pyrrole, could possibly give rise to the slowly varying distribution of N−H frequencies. The variance in frequency, or inhomogeneous width, corresponding to A_2 and which averages on the time scale of 4.4 ps, is 6.3 cm^{-1}. The spectral diffusion we measure would then be attributed to structural relaxation from changes in many body interactions in clusters of solvent molecules above and below the molecular plane. However, with pyrrole the N−H interactions with solvent must also be considered, although any such structures would be likely to break up during the process of rotational diffusion about the axis perpendicular to the plane.

Of great interest will be the dynamics of N−H modes undergoing hydrogen-bonding interactions. Examples of this that are accessible to ultrafast infrared spectroscopic methods include proteins and peptides as well as liquids, and these will form our future work, building on the baseline measurements reported here of N−H modes in a relatively inert environment.

Acknowledgment. This research was supported by grants from the NIH (GM12592) and NSF with instrumentation from the NIH Resource Grant PHS 41 RR03148.

References and Notes

(1) Schotte, F.; Anfinrud, P. A.; Wulff, M. *Trends Opt. Photonics* **2002**, *72*, 31.

(2) Schoenlin, R. W.; Chong, H. H. W.; Glover, T. E.; Heimann, P. A.; Leemans, W. P.; Padmore, H. A.; Shank, C. V.; Zholents, A. A.; Zolotorev, M. S.; Corlett, J. S. *C. R. Acad. Sci., Ser. IV: Phys., Astrophys.* **2001**, *2*, 1373.

(3) Moffat, K. *Faraday Discuss.* **2002**, *122*, 65.

(4) Prompers, J. J.; Brueschweiler, R. *J. Am. Chem. Soc.* **2002**, *124*, 4522.

(5) Hamm, P.; Lim, M.; Hochstrasser, R. M. *J. Phys. Chem. B* **1998**, *102*, 6123.

(6) Hamm, P.; Lim, M.; DeGrado, W. F.; Hochstrasser, R. M. *Proc. Natl. Acad. Sci. U.S.A.* **1999**, *96*, 2036.

(7) Asplund, M. C.; Zanni, M. T.; Hochstrasser, R. M. *Proc. Natl. Acad. Sci. U.S.A.* **2000**, *97*, 8219.

(8) Hamm, P.; Lim, M.; DeGrado, W. F.; Hochstrasser, R. M. *J. Chem. Phys.* **2000**, *112*, 1907.

(9) Woutersen, S.; Hamm, P. *J. Phys. Chem. B* **2000**, *104*, 11316.

(10) Zanni, M. T.; Ge, N.-H.; Kim, Y. S.; Hochstrasser, R. M. *Proc. Natl. Acad. Sci. U.S.A.* **2001**, *98*, 11265.

(11) Zanni, M. T.; Asplund, M. C.; Hochstrasser, R. M. *J. Chem. Phys.* **2001**, *114*, 4579.

(12) Zanni, M. T.; Gnanakaran, S.; Stenger, J.; Hochstrasser, R. M. *J. Phys. Chem. B* **2001**, *105*, 6520.

(13) Golonzka, O.; Khalil, M.; Demirdoven, N.; Tokmakoff, A. *Phys. Rev. Lett.* **2001**, *86*, 2154.

(14) Hamm, P.; Hochstrasser, R. M. In *Ultrafast Infrared and Raman Spectroscopy*; Fayer, M. D., Ed.; Marcel Dekker Inc.: New York, 2001; p 273.

(15) Woutersen, S.; Hamm, P. *J. Chem. Phys.* **2001**, *115*, 7737.

(16) Woutersen, S.; Mu, Y.; Stock, G.; Hamm, P. *Proc. Natl. Acad. Sci. U.S.A.* **2001**, *98*, 11254.

(17) Ge, N.-H.; Zanni, M. T.; Hochstrasser, R. M. *J. Phys. Chem. A* **2002**, *106*, 962.

(18) Stenger, J.; Madsen, D.; Dreyer, J.; Hamm, P.; Nibbering, E. T. J.; Elsaesser, T. *Chem. Phys. Lett.* **2002**, *354*, 256.

(19) Rubtsov, I. V.; Wang, J.; Hochstrasser, R. M. *J. Phys. Chem. A* **2003**, *107*, 3384.

(20) Rubtsov, I. V.; Hochstrasser, R. M. *J. Phys. Chem. B* **2002**, *106*, 9165.

(21) Khalil, M.; Demirdoven, N.; Tokmakoff, A. *Phys. Rev. Lett.* **2003**, *90*, 047401/1.

(22) Rubtsov, I. V.; Wang, J.; Hochstrasser, R. M. *Proc. Natl. Acad. Sci. U.S.A.* **2003**, *100*, 5601.

(23) Hamm, P.; Lim, M.; Hochstrasser, R. M. *Phys. Rev. Lett.* **1998**, *81*, 5326.

(24) Okumura, K.; Tokmakoff, A.; Tanimura, Y. *Chem. Phys. Lett.* **1999**, *314*, 488.

(25) Lim, M.; Hamm, P.; Hochstrasser, R. M. *Proc. Natl. Acad. Sci. U.S.A.* **1998**, *95*, 15315.

(26) de Boeij, W. P.; Pshenichnikov, M. S.; Wiersma, D. A. *Chem. Phys. Lett.* **1996**, *253*, 53.

(27) Demirdoven, N.; Khalil, M.; Tokmakoff, A. *Phys. Rev. Lett.* **2002**, *89*, 237401/1.

(28) Tokmakoff, A.; Urdahl, R. S.; Zimdars, D.; Francis, R. S.; Kwok, A. S.; Fayer, M. D. *J. Chem. Phys.* **1995**, *102*, 3919.

(29) Stenger, J.; Madsen, D.; Hamm, P.; Nibbering, E. T. J.; Elsaesser, T. *J. Phys. Chem. A* **2002**, *106*, 2341.

(30) Gallot, G.; Bratos, S.; Pommeret, S.; Lascoux, N.; Leicknam, J. C.; Kozinski, M.; Amir, W.; Gale, G. M. *J. Chem. Phys.* **2002**, *117*, 11301.

(31) Lee, S.-H.; Mirkin, N. G.; Krimm, S. *Biopolymers* **1999**, *49*, 195.

(32) Grubbs, W. T.; Dougherty, T. P.; Heilweil, E. J. *J. Phys. Chem.* **1995**, *99*, 10716.

(33) Wynne, K.; Galli, C.; Hochstrasser, R. M. *Chem. Phys. Lett.* **1992**, *193*, 17.

(34) Ambroseo, J. R.; Hochstrasser, R. M. *J. Chem. Phys.* **1988**, *89*, 5956.

(35) Munoz-Crego, C.; Santamaria, J. *Chem. Phys.* **1997**, *224*, 215.

(36) Mukamel, S. *Principles of nonlinear optical spectroscopy*; Oxford University Press: New York, 1995.

(37) Ge, N.-H.; Hochstrasser, R. M. *PhysChemComm* ***2002***, *5*(3), 17−28.

(38) Lim, M.; Hochstrasser, R. M. *J. Chem. Phys.* **2001**, *115*, 7629.

(39) Yee, T. K.; Gustafson, T. K. *Phys. Rev.* **1978**, *18*, 1597.

(40) Oxtoby, D. W.; Levesque, D.; Weis, J. J. *J. Chem. Phys.* **1978**, *68*, 5528.

(41) Kubo, R. *Adv. Chem. Phys.* **1969**, *15*, 101.

(42) Asplund, M. C.; Lim, M.; Hochstrasser, R. M. *Chem. Phys. Lett.* **2000**, *323*, 269.

(43) Piryatinski, A.; Skinner, J. L. *J. Phys. Chem. B* **2002**, *106*, 8055.

(44) Yu, J.-Y.; Nagasawa, Y.; van Grondelle, R.; Fleming, G. R. *Chem. Phys. Lett.* **1997**, *280*, 404.

(45) Mellouki, A.; Georges, R.; Herman, M.; Snavely, D. L.; Leytner, S. *Chem. Phys.* **1997**, *220*, 311.

(46) Snavely, D. L.; Blackburn, F. R.; Ranasinghe, Y.; Walters, V. A.; Gonzalez del Riego, M. *J. Phys. Chem.* **1992**, *96*, 3599.

(47) Held, A.; Herman, M. *Chem. Phys.* **1995**, *190*, 407.

(48) Mellouki, A.; Lievin, J.; Herman, M. *Chem. Phys.* **2001**, *271*, 239.

(49) Youngren, G. K.; Acrivos, A. *J. Chem. Phys.* **1975**, *63*, 3846.

(50) Sension, R. J.; Hochstrasser, R. M. *J. Chem. Phys.* **1993**, *98*, 2490.

(51) Myers, A. B.; Pereira, M. A.; Holt, P. L.; Hochstrasser, R. M. *J. Chem. Phys.* **1987**, *86*, 5146.

(52) Diraison, M.; Guissani, Y.; Leicknam, J. C.; Bratos, S. *Chem. Phys. Lett.* **1996**, *258*, 348.

(53) O'Reilly, D. E.; Schacher, G. E. *J. Chem. Phys.* **1963**, *39*, 1768.

(54) Bartoli, F. J.; Litovitz, T. A. *J. Chem. Phys.* **1972**, *56*, 404.

(55) Nakagawa, T.; Yamanaka, S.; Urakawa, H.; Kajiwara, K.; Maeda, H.; Hayashi, S. *J. Mol. Liq.* **1998**, *75*, 127.

(56) Soetens, J.-C.; Jansen, G.; Millot, C. *Mol. Phys.* **1999**, *96*, 1003.

(57) Larsen, D. S.; Ohta, K.; Fleming, G. R. *J. Chem. Phys.* **1999**, *111*, 8970.

(58) Laaksonen, A.; Stilbs, P.; Wasylishen, R. E. *J. Chem. Phys.* **1998**, *108*, 455.

(59) Tsuzuki, S.; Honda, K.; Uchimaru, T.; Mikami, M.; Tanabe, K. *J. Phys. Chem. A* **2002**, *106*, 4423.